Requirements for *Arabidopsis ATARP2* and *ATARP3* during Epidermal Development

Jie Le, Salah El-Din El-Assal, Dipanwita Basu,
Mohamed E. Saad, and Daniel B. Szymanski*
Agronomy Department
Purdue University
Lily Hall
915 West State Street
West Lafayette, Indiana 47907-2054

Summary

Plant cells employ the actin cytoskeleton to stably position organelles, as tracks for long distance transport, and to reorganize the cytoplasm in response to developmental and environmental cues [1]. While diverse classes of actin binding proteins have been implicated in growth control, the mechanisms of cytoskeletal reorganization and the cellular functions of specific actin filament arrays are unclear. *Arabidopsis* trichome morphogenesis includes distinct requirements for the microtubule and actin filament cytoskeletons. It also is a genetically tractable process that is providing new knowledge about cytoskeleton function in plants [2]. The "distorted group" of mutants defines a class of at least eight genes that are required during the actin-dependent phase of trichome growth. Using map-based cloning and a candidate gene approach, we identified mutations in *ARP3* (*ATARP3*) and *ARP2* (*ATARP2*) genes as the cause of the *distorted1* (*dis1*) and *wurm* (*wrm*) phenotypes, respectively. ARP2 and ARP3 are components of the evolutionarily conserved ARP2/3 complex that nucleates actin filament polymerization [3]. Mutations in *DIS1* and *WRM* caused severe trichome growth defects but had relatively mild effects on shoot development. *DIS1* rescued the phenotype of Δ*arp3* when overexpressed in *S. cerevisiae*. Developing *dis1* trichomes had defects in cytoplasmic actin bundle organization and reduced relative amounts of cytoplasmic actin filaments in developing branches.

Results and Discussion

Branch position, shape, and number are tightly regulated during wild-type trichome development [4]. Wild-type trichomes in the process of branch formation (stage 3) and one that recently completed branching (stage 4) are labeled in Figure 1A. Most of the cell volume is generated during a massive cell expansion phase (stage 5) that occurs after branch initiation is complete. Trichome shape on *dis1* leaves was indistinguishable from that of the wild-type through stage 3, but subsequently, the trichomes were swollen, twisted, and often had a reduced branch length (Figure 1B). Recessive *dis1*, *wrm*, and *gnarled* (*grl*) mutations cause indistinguishable stage-specific swelling [4, 5], and each of the *dis1* and *wrm* alleles described in this paper also had the same

*Correspondence: dszyman@purdue.edu

stage-specific swelling and reduced branch elongation defects (data not shown). Because *dis1-1* was a predicted null allele of *DIS1* (see below), we used this allele for all of our detailed phenotypic characterizations. Measurements with scanning electron microscopy (SEM) demonstrated that 40% (n = 43) of *dis1-1* stage 4 trichomes had a cell diameter of more than 30 μm. In the wild-type, a stage 4 cell diameter exceeding 30 μm was not observed in either this (n = 45) or previous studies [4]. During stage 6, papillae or tubercles decorate the surface of highly expanded trichomes. Papillae on the stalks of wild-type trichomes were slightly oval and varied in length from ∼1.5 μm to ∼3 μm (Figure 1C). In mature *dis1* trichomes, papillae at the tips of abortive branches were often absent (Figure 1D). In obviously swollen regions of the stalk, papillae up to ∼9 μm in length were common. Equivalently sized papillae were not observed in the wild-type. In both mutant and wild-type cells, the long axis of the papillae and the cell were aligned. Presumably, the orientation of the papillae reflected some aspect of polarized growth that was maintained in the mutant. Pavement cells are another highly polarized cell type that appear to utilize both microtubule and actin-filament structures during morphogenesis [6]. At 12 days after germination (DAG), wild-type pavement cells located in the distal 1/3 of the cotyledon were highly lobed (Figure 1E). Some *dis1* cotyledon pavement cells at comparable positions were highly lobed (Figure 1F). Other *dis1* pavement cells in the same region of the identical cotyledon had reduced lobe expansion (Figure 1G). *dis1-T1* pavement cells displayed similar phenotypes (data not shown). We have no explanation for this patchy phenotype. *dis1* pavement cells consistently failed to adhere normally, and gaps between adjacent cells were frequently detected (Figures 1F and 1G).

With the exception of the striking trichome phenotype, the whole plant architecture of *dis1* and *wrm* plants was very similar to that of the wild-type (Figures 1H–1J). However, shoot fresh weight accumulation of *dis1-1* and phenotypically wild-type siblings differed at 15 DAG. In one representative experiment, the mean *dis1* shoot weight (75 ± 9 mg [n = 6]) was reduced by 35% compared to the wild-type (117 ± 9 mg [n = 6]). The phenotypes are consistent with the detection of *DIS1* transcript in roots and leaves [7]. Despite the clear actin-dependent growth of root hairs [8], *dis1* root hairs were very similar to those of the wild-type (data not shown). Pollen germination and tip growth did not require *DIS1* or *WRM*, because all of the alleles examined in this study were efficiently transmitted through pollen and *dis1* and *wrm* plants yielded thousands of seeds. However, these results do not preclude a subtle or conditional effect of *DIS1* or *WRM* on pollen development.

To identify the affected genes, we initiated map-based cloning of *DIS1*. Consistent with its published position on the classical map [9], *dis1* mapped between T28P6 and F9L1 on the upper arm of chromosome 1 (Figure 2A). Unfortunately, in mapping populations that em-
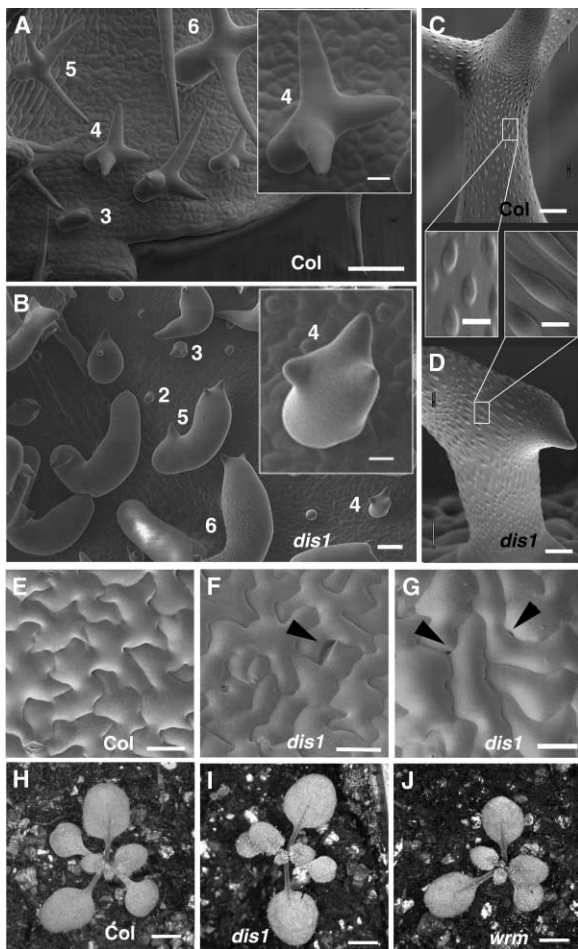
Figure 1. Trichome, Pavement Cell, and Shoot Phenotypes of Wild-Type, *dis*, and *wrm* Seedlings

(A) The upper surface of developing leaves of wild-type. Inset, higher magnification view of a stage 4 trichome.

(B) The upper surface of developing leaves of *dis1*. Inset, higher magnification view of a stage 4 trichome.

(C) Papillae on mature wild-type trichomes.

(D) Papillae on mature *dis1* trichomes; middle panel, higher magnifications of regions from (C) and (D).

(E) The upper surface of 12 DAG wild-type cotyledon pavements cells.

(F and G) The upper surface of 12 DAG *dis1* cotyledon pavements cells.

(H) A wild-type seedling (11 DAG).

(I) A *dis1* seedling (11 DAG).

(J) A *wrm* seedling (11 DAG).

The scale bars represent 50 μm in (A) and (B), 10 μm in the insets of (A) and (B), 10 μm in (C) and (D), 2 μm in the insets of (C) and (D), 50 μm in (E)–(G), and 2 mm in (H)–(J). The stage of an individual trichome is labeled with a number. The arrowheads indicate the gaps between adjacent pavement cells.
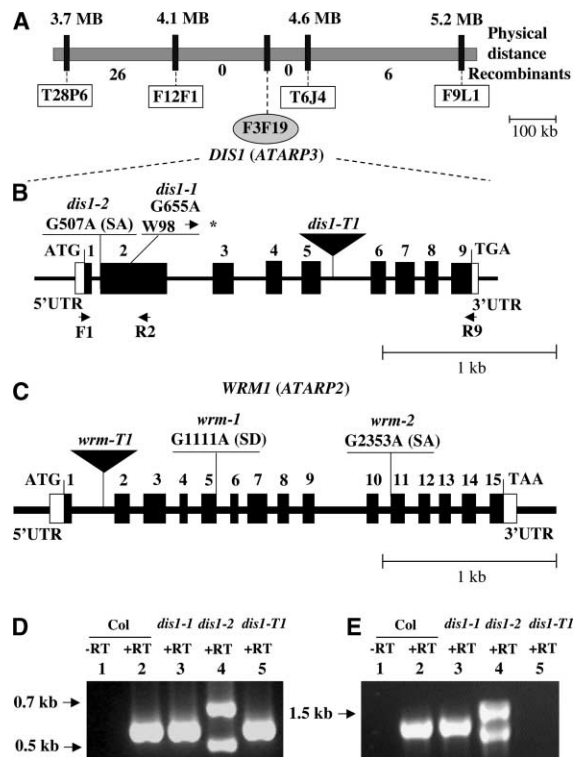

Figure 2. Mapping and Molecular Characterization of *DIS1* and *WRM* Mutant Alleles

(A) The mapping interval of the *DIS1* gene. The boxes indicate the molecular marker, and the oval represents *DIS1*-containing BAC (F3F19). The recombinant frequency for each marker is given.

(B) The physical structure of the *DIS1* gene. Exons are represented by closed rectangles, and introns are represented by lines. F1, R2, and R9 are PCR primers. The *dis1-1*, *dis1-2*, and *dis1-T1* alleles are defined.

(C) The physical structure of the *WRM* gene. The *wrm-1*, *wrm-2*, and *wrm-T1* alleles are defined.

(D and E) RT-PCR analysis of the *DIS1* mRNA in wild-type and mutant backgrounds. (D) RT-PCR using primers F1 and R2. (E) RT-PCR using primers F1 and R9. Lane 1, no (−) reverse transcriptase (RT) wild-type; lane 2, Plus (+) RT wild-type; lane 3, *dis1-1* (+RT); lane 4, *dis1-2* (+RT); lane 5, *dis1-T1* (+RT).

ployed the *dis1-1* allele, we failed to detect recombination within a 500 kb interval that was expected to contain *DIS1* (0 recombinants/1012 chromosomes). *ATARP3* [7] is located within our mapping interval on chromosome 1. *wrm* also mapped to a region of chromosome 3 that contains *ATARP2* ([5], D.B.S., unpublished data). Therefore, we tested the ability of publicly available Salk T-DNA insertions into *ATARP3* and *ATARP2* to cause a

distorted trichome phenotype. Salk_010045 contained an insertion in the *ATARP3* gene, and lines homozygous for the insertion displayed a completely penetrant, distorted trichome phenotype that was indistinguishable from *dis1-1*. Progeny from hemizygous Salk_010045 plants segregated for the trichome phenotype. All F$_1$ plants derived from crosses between *dis1-1* (n = 24), *dis1-2* (n = 29), and Salk_010045 were mutant. Therefore Salk_010045 was allelic to *dis1-1* and *dis1-2* and was renamed *dis1-T1*. We wanted to determine if the *ATARP3* gene sequence was altered in *dis1-1* and *dis1-2*. *dis1-1* was originally isolated in the *Landsberg erecta* (*Ler*) background, and *dis1-2* was originally isolated in Columbia-O (Col). Compared to the *Ler* sequence, *dis1-1* had a single nucleotide change that introduced a nonsense mutation at amino acid 98 (W98*) (Figures 2B and S1 [in the Supplemental Data available with this article online]). The *dis1-2* allele eliminated a consensus splice acceptor sequence of intron 1 (Figure

Table 1. Amino Acid Sequence Comparisons between Predicted *Arabidopsis* ARP2/3 Complex Components and Homologs in Human and *S. cerevisiae*

Arabidopsis Gene[a]	Human: Ident. % (Sim. %)	Yeast: Ident. % (Sim. %)
ATARP2[b]	61 (79)	56 (74)
ATARP3[b]	56 (71)	51 (63)
ATARPC1A[b]	42 (59)	34 (51)
ATARPC1B[b]	42 (61)	34 (51)
ATARPC2A[b]	26 (46)	28 (47)
ATARPC2B[b]	29 (47)	23 (44)
ATARPC3[b]	47 (66)	39 (58)
ATARPC4	65 (81)	59 (74)
ATARPC5[b]	32 (53)	23 (45)

[a] Named according to Human Genome Organization conventions.
[b] Supported by mRNA sequence data.

Figure 3. *Arabidopsis DIS1* Can Complement the Growth Defects of *S. cereviseae* Δ*arp3*

(A) Left, *S. cereviseae* patches of haploid wild-type strain BY4741 (above) and untransformed Δ*arp3* (below); right, patches of Δ*arp3* transformed with pYDIS1 (above) and pDEST52 (below). All strains were grown on glucose-containing plates.
(B) Same strains as those in (A), but struck on galactose inducer-containing plates.

2B). The sequencing results from three independent *dis1* alleles, and their failure to complement each other provided very strong evidence that *DIS1* and *ATARP3* were the same gene.

SALK_003448 contained a T-DNA insertion in the first intron of *ATARP2* (Figure 1C). Lines homozygous for SALK_003448 had a distorted trichome phenotype. When crossed with *wrm-1* (n = 35) and *wrm-2* (n=15), homozygous SALK_003448 plants failed to complement. Based on these allelism tests, SALK_003448 is referred to as *wrm-T1*. Sequencing the *ATARP2* gene in the *wrm-1* and *wrm-2* backgrounds identified single nucleotide changes at the +1 position of the consensus splice donor following exon 5 and at the −1 position of the consensus splice acceptor preceding exon 11, respectively (Figure 2C). The molecular genetic characterization of three independent *wrm* alleles provided strong evidence that *WRM* corresponded to *ATARP2*. Although indisputable proof that *DIS1* encodes *ATARP3* and *WRM* encodes *ATARP2* requires transformation of the mutants with wild-type gene sequences and phenotypic rescue, we will refer to *ATARP3* as *DIS1* and *ATARP2* as *WRM* for the remainder of this paper.

Full-length cDNA sequences for *DIS1* and *WRM* are in GenBank [7, 10]. Predicted *DIS1* and *WRM* polypeptides shared an overall identity of more than ∼50% with yeast and human ARP3 and ARP2 homologs, respectively (Table 1), and many of the amino acids that bind nucleotide and profilin are also conserved in *DIS1* and *WRM* (Figures S1 and S2, available in the Supplemental Data). Of the 50 additional amino acids that *DIS1* encoded compared to conventional actins, 40 of them were distributed among 4 "insert" positions that were identified in the *Bos taurus* ARP2/3 crystal structure [11] (Figure S1). Structure predictions [12] and the solved structure of the ARP2/3 complex suggest that the barbed end of ARP3 makes contacts with the pointed end of ARP2. The key barbed end residues of *DIS1*, like those of other ARP3s, closely resembled actin [12, 13]. Pointed end residues of actin that interact with the barbed end of adjacent subunits were not highly conserved in *DIS1* or other ARP3s, but they were conserved in *WRM* and other ARP2s (Figures S1 and S2). Despite the striking level of identity between *DIS1* and other ARP3s, two human, an *Acanthamoeba*, and *Dictyostelium* anti-ARP3
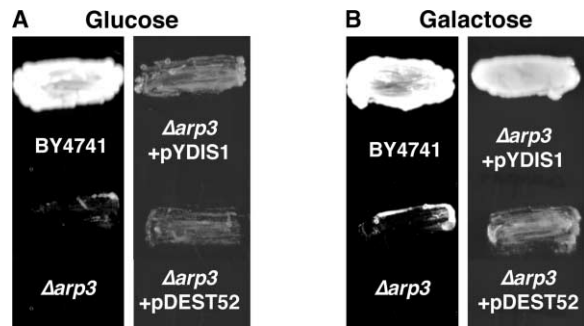
antibodies [12, 14–16] failed to recognize either recombinant or endogenous DIS1 (data not shown).

Because both *dis1-1* and *dis1-2* were candidate null alleles, we characterized them in more detail. *dis1-2* contained a single G-to-A change at the −1 splice acceptor site of intron 1. Based on the DNA sequence of the RT-PCR products, this mutation caused both the failure to splice intron 1 (Figures 2D and 2E, lane 4, upper band) and the use of a cryptic acceptor at +56 in exon 2 (Figures 2D and 2E, lane 4, lower band). The RT-PCR signal for wild-type (Figure 2D, lanes 1 and 2) and each of the *dis1* alleles (data not shown) required reverse transcriptase activity and therefore was derived from mRNA. The unspliced and misspliced *dis1-2* mRNAs encoded 16 correct amino acids before the reading frame shifted to nonsense, and soon thereafter, stop codons were present in all reading frames. The T-DNA insertion in *dis1-T1* was likely to prematurely terminate the *ATARP3* transcript, as the mRNA was detected with primers upstream (Figure 2D, lane 5), but not downstream (Figure 2E, lane 5), from the T-DNA.

We tested the ability of *DIS1* to function as an *ARP3* in *S. cerevisiae*. Yeast strains with mutations in the *ARP3* gene display severe growth defects [17, 18]. Δ*arp3* haploid cells were slow growing compared to wild-type isogenic lines (Figure 3). The slow growth phenotype was not rescued when either the empty vector (Δ*arp3* + pDEST52) or *DIS1*-expressing (Δ*arp3* + pYDIS1) strains were grown on noninducing medium (Figure 3A). When grown on inducing media, the Δ*arp3* + pYDIS1 strains exhibited wild-type growth compared to the empty vector control (Figure 3B). The percentage of unseparated cells was reduced from 3.5% (n = 263; Δ*arp3* + pDEST52) to 0.5% (n = 503; Δ*arp3* + pYDIS1) when grown in inducing medium. These data demonstrated the ability of *DIS1* to function as an *ARP3* in the context of a well-characterized ARP2/3 complex [17].

To begin to test the hypothesis that *DIS1* is directly involved in the generation or organization of actin filaments during trichome morphogenesis, we analyzed the actin cytoskeleton in *dis1* and wild-type trichomes at the onset of the *dis1* phenotype during branch elongation.
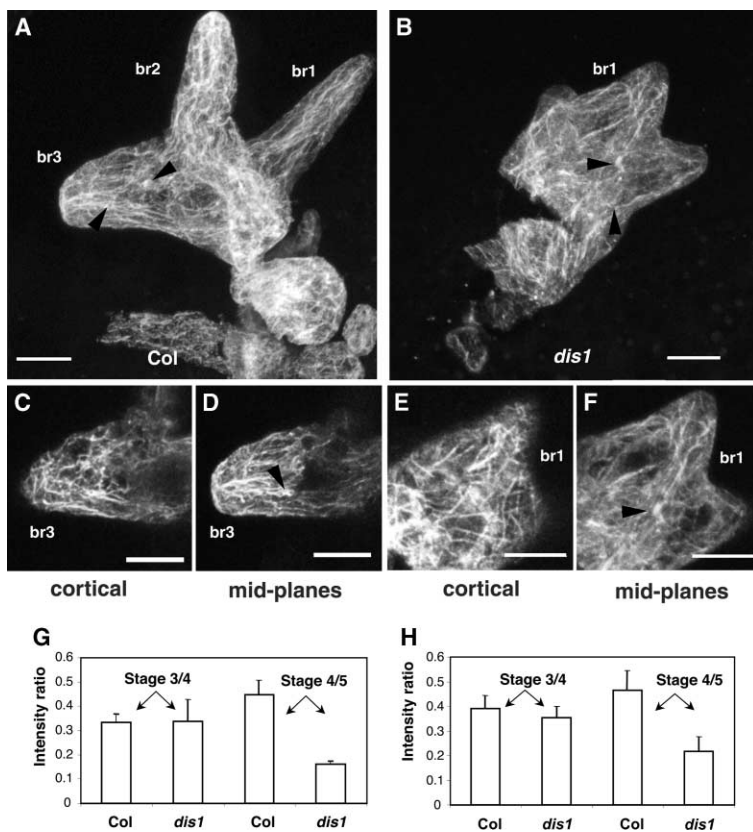
Figure 4. Actin Phenotypes of *dis1* Trichomes

(A) Wild-type, fractured cell, maximum projection of all planes. br1, oldest branch; br2, second oldest branch; br3, oldest branch.
(B) *dis1*, fractured cell, maximum projection of all planes. br1, oldest branch.
(C and D) Higher magnification of br3 from (A).
(E and F) Higher magnification of br1 from (B).
(C) and (E) are maximum projections of cortical planes; (D) and (F) are maximum projections of cytoplasmic midplanes.
(G and H) Ratio of the core cytoplasmic F-actin signal to the total cytoplasmic F-actin signal in developing branches. (G) Ratios with anti-actin antibody N350. (H) Ratios with Alexa 488 Phalloidin. The values are the mean ratios ± standard deviation from 5–10 branches.
The arrowheads indicate the cytoplasmic bundles that extend toward the branch tip. The scale bars represent 10 μm.

Because overexpression of talin-GFP in trichomes leads to excessive actin filament bundling [19], freeze shattering of fixed samples and live cell phalloidin uptake were used to localize actin. Both methods revealed similar patterns of cytoplasmic and cortical filaments or bundles, but the antibody results, which consistently detected finer actin filaments, are shown here. The stalks and branches of stage 4 wild-type and *dis1* trichomes contained a dense meshwork of cortical and cytoplasmic filaments (Figures 4A and 4B). The cortical cytoskeleton in similarly staged *dis1* branches (Figure 4E) did not differ noticeably from the wild-type (Figure 4C). In wild-type trichomes, many cytoplasmic bundles ∼10–15 μm in length extended toward the branch apex and coalesced in actin-rich distal structures near the branch apex (Figure 4D and Figures S3A and S3C, available in the Supplemental Data). As the branches elongated to ∼20–45 μm, seemingly continuous bundles extended along its entire length (see br1, Figure 4A). In developing *dis1* branches, cytoplasmic filaments or bundles were abundant, but they failed to localize as coherent populations that were aligned with the long axis of the branch. Instead, bundles often extended between the branch tip and seemingly random locations in the stalk cytoplasm, or, in many cases, from cortical locations (Figures 4B and 4F). Similar defects occur in stage 4 *grl* cells [4]. Because of the density of actin filaments in both mutant and wild-type trichomes, we were not able to analyze possible differences in filament branching. At later stages of development, abnormally thick actin bundles were occasionally observed in *dis1* stalks and branches (Figure S3D).

We wanted to determine if there were any differences in the relative amounts of cytoplasmic actin filaments in mutant and wild-type branches. To minimize the contribution of abortive *dis1* branches, only *dis1* trichomes with stalks less than 50 μm were used. We measured the relative amounts of "core" cytoplasmic F-actin to total cytoplasmic F-actin in stage 3/4 (st3/4) and stage 4/5 (st4/5) branches (see the Experimental Procedures). Because of cell-to-cell variation in the efficiency of actin filament labeling and therefore differences in imaging settings, we used the total actin filament signal within a branch subregion as an internal standard for quantitation. The antibody and phalloidin signal came primarily from filaments, because the signal from Latrunculin B (LatB)-treated samples was at or near background (data not shown). The ratio of the "core" to total cytoplasmic fluorescence signal was calculated by using both antibody (Figure 4G) and phalloidin (Figure 4H) probes. As an example of the input data, representative maximum projections of cortical (Figure S3, left) and core cytoplasmic regions (Figure S3, middle) are included in the Supplemental Data available with this article online. Representative transverse sections of st3/4 and st4/5 branches with regions of interest for intensity measurements are also displayed in Figures S3A–S3D (right). The relative ratios of the core cytoplasmic F-actin signal to the total F-actin signal in wild-type and *dis1* st3/4 branches were not significantly different. Relative core F-actin levels in wild-type st4/5 branches were slightly elevated compared to those in st3/4 branches (Figures 4G and 4H). The relative amount of F-actin in st4/5 *dis1* branches was reduced compared to st3/4 and st4/5

wild-type as well as st3/4 *dis1* branches (Figures 4G and 4H). Presently, we cannot determine if this reduction was attributable directly to stage-specific effects of *DIS1* on actin filaments and/or the indirect effects of reduced branch growth and altered cytoplasmic organization.

If *DIS1* and *WRM* encode components of a functional ARP2/3 complex, other subunits of the complex should be encoded by the *Arabidopsis* genome. Using the amino acid sequences of the human and yeast ARP2/3 complex proteins in BLASTp queries, homologs of six of the seven subunits were found and are supported by mRNA sequence (Table 1). Two copies of an *ARPC1* (p40) gene were present: *ATARPC1A* (At2g30910) and *ATARPC1B* (At2g31300). *ARPC2* (p34/p35) was encoded by two genes: *ATARPC2A* on chromosome 1 and *ATARPC2B* on chromosome 2. *ARPC3* (p21) and *ARPC5* (p16) homologs were encoded by *ATARPC3* and *ATARPC5*, respectively. An *ARPC4* (p19/p20)-encoding sequence is present in the *Arabidopsis* sequence, but it has been misannotated both as a partial protein fusion to a kinesin-like protein (GenBank accessions: H71402 and CAB10194) on chromosome 4 and as intergenic DNA. A full-length cDNA sequence in the database (GenBank accession: NM_117492) proves that *ATARPC4* is not part of the kinesin-like transcript. Using a predicted *ARPC4* from rice and a known human ARPC4, a TBLASTN search identified putative *ARPC4*-encoding exons. We used multiple sequence alignments (between a preliminary *ATARPC4*-encoded polypeptide and *ARPC4* amino acid sequences from rice, human, and yeast) in conjunction with *Arabidopsis* splice donor and acceptor probability tables to generate a refined, predicted *ATARP4* polypeptide that was ~60% identical to both human and yeast *ARPC4* (Table 1).

In this paper, we showed that *DIS1* and *WRM* encode *Arabidopsis* homologs of ARP3 and ARP2, respectively. In non-plant cells, the ARP2/3 complex nucleates actin filaments from the sides of existing filaments [20, 21]. There is strong evidence that ARP2/3-dependent nucleation is directly linked with its functions in the cell during membrane protrusion or organelle motility [22]. If *DIS1* and *WRM* function like known ARP3s and ARP2s, they are likely to regulate multiple processes such as membrane trafficking, organelle motility, and the generation of specific actin filament arrays [22, 23]. Actin localization experiments in stage 4 wild-type and *dis1* trichomes provides some clues as to the mechanism of *DIS1* function in the context of actin bundle formation. In the wild-type, both the location of filament nucleation and their higher order organization are tightly regulated. Stage 4 trichomes contain a dense population of core cytoplasmic bundles, a subset of which are aligned with the long axis of the branch and terminate near unknown membrane compartments (Figure 4). These regions of concentrated actin filament ends may reflect membrane surfaces that either nucleate or capture filaments in order to position the endomembrane system for persistent polarized growth during branch elongation. A failure to generate or position the endomembrane system for polarized organelle and vesicle trafficking into the branch might explain the mislocalized expansion of *dis1* trichome stalks, instead of branches, during the transition to actin-dependent growth. In *dis1* trichomes, the core

cytoplasmic bundles are disorganized and are reduced in amount relative to total cytoplasmic filaments (Figure 4). A simplistic mechanism of bundle formation may include *DIS1*-independent nucleation, *DIS1*-dependent branching of actin filaments, and the activity of a bundling protein that "zippers" filaments into stable and oriented bundles. The coordinated activity of ARP2/3-dependent branching and FASCIN-dependent bundling can generate actin bundles [24]. Although *Arabidopsis* does not encode a FASCIN homolog, it may employ proteins with multiple predicted actin binding domains such as FIMBRIN [25] or VILLIN [26] to generate bundles. The thick actin bundles observed in st4/5 and later *dis1* trichomes could reflect an imbalance in the filament nucleating, branching, and bundling activities in cells.

The pleiotropic, but mild phenotypes of *dis1* plants differ greatly from the lethality and severe growth defects observed when *ARP3* activity is eliminated in animal and yeast cells. Mutations in *Drosophila ARP3* cause sterility and embryo lethality (but no significant effects on sensory bristle morphology) [27]. *ARP3* gene deletions are lethal in *S. pombe* [28] and cause severely reduced growth rates in *S. cerevisiae* [17]. If *DIS1* functions as part of an ARP2/3 complex, *dis1-1* plants may not be null for complex activity. In *S. cerevisiae*, only Δarc40 (*ARPC1*) is lethal, and partially assembled ARP2/3 complexes can be isolated from Δarp3 strains [17]. It seems more likely that the mild *dis1* phenotypes and the extensive actin cytoskeletons that are present in a variety of *dis1* cell types (D.B.S., unpublished data) arise from a *DIS1*-independent nucleating activity. FORMINs are a newly discovered class of actin filament-nucleating proteins [29, 30]. *Arabidopsis* encodes at least 21 predicted FORMIN-like genes, 11 of which contain a predicted signal sequence and a membrane-spanning segment [31]. Perhaps FORMINs function redundantly as the major actin filament nucleators in *Arabidopsis*, and ARP2/3 plays a secondary role that is easily identified in trichomes, which have highly constrained requirements for actin-containing structures.

In animal cells, ARP2/3-dependent filament nucleation drives plasma membrane protrusion and local cell outgrowth. In walled plant cells that use turgor pressure to expand, an ARP2/3 complex may have other roles in the generation of stable transvacuolar cytoplasm, organelle dynamics, and endocytosis. The potential roles of *DIS1* and *WRM* in actin filament nucleation and force generation in plant cells can be examined further by using the single cell system of trichome development. Parallel analyses of the trichome, tissue, and organ phenotypes of *dis1* and *wrm* will increase our knowledge about the general plant functions of ARP2 and ARP3, and perhaps the ARP2/3 complex. It is now essential to develop strategies to isolate an ARP2/3 complex in plants to determine if the plant ARP2/3 complex forms branched actin filaments, how it is activated, and its function in growing cells.

Experimental Procedures

Strains and Growth Conditions
Mutant L*er dis1-1* [9] was obtained from the *Arabidopsis* stock center and was outcrossed to Col five times prior to use. *dis1-2* and

wrm-2 were recovered from an EMS-mutagenized Col population by using standard protocols. *wrm-1* (*Ler*) was a gift from M. Hulskamp and was outcrossed to Col five times prior to use. For SEM and fresh weight measurements, seedlings were grown in soil under continuous illumination at 25°C.

Cytoskeleton Localization and Quantification
Antibody labeling was done as described in [4]. For phalloidin staining, tissues were incubated in 0.198 μM Alexa Fluor 488 phalloidin (Molecular Probes) in 100 mM PIPES-KOH, 5 mM EGTA, 4 mM $MgCl_2$ (pH 6.9) (PEM) containing 1% glycerol for 45–100 min. For F-actin quantification, some samples were fixed in 2% formaldehyde in buffer and were then incubated in Alexa Fluor 488 phalloidin and PEM overnight. Confocal images were collected by using an MRC Bio-Rad 2100 confocal microscope and were analyzed with Meta-Morph software (Universal Imaging). Nikon 60× Plan Apo (NA 1.2) water immersion and 100× Plan Apo (NA 1.4) oil immersion objectives were used.

To quantify the relative amount of core cytoplasmic actin filaments to total actin filaments in developing trichomes, branches with the long axis parallel to the *xy* plane were chosen. Image stacks were rotated to orient the branch direction parallel to the *x* or *y* axis to generate orthogonal views (*yz* or *xz*). These transverse views were used for relative actin filament quantification. Branches with lengths between 10 and 15 μm were defined as stage 3/4. Branches with lengths between 16 and 50 μm were defined as stage 4/5. To standardize the region of measurement among samples, the position of the middle orthogonal plane of each branch was defined at 1/2 of the total branch length (1/2L). For each branch, transverse sections 1.3 μm distal and proximal from the 1/2L plane were quantified. Based on the consistent disappearance of cortical filaments beyond a distance of 2.5 μm from the plasma membrane, a 2.5 μm wide ring around the perimeter of each transverse section was defined as "cortical" cytoplasm. Cytoplasmic space not included within the outer 2.5 μm ring was defined as "core" cytoplasm (for example images, see Figure S3). Total cytoplasmic space was the "core" plus "cortical." Total integrated fluorescence intensity was measured within the core and total cytoplasmic space, and the ratio of the core to total cytoplasmic signal was calculated for each transverse slice. Between 15 and 20 planes were measured and averaged for each branch. The values for each stage were computed from 5–10 branches.

***S. cereviseae Δarp3* Complementation**
The *S. cereviseae* Arp3 deletion was obtained from Resgen (Invitrogen). The 1283 bp cDNA region of *DIS1* was amplified by using the primers 5′-CACCATAATGGATCCGACTTCTCGACCCGC-3′ and 5′-TCAATATCATTCCCTTGAACACCGG-3′, cloned into the pENTR/D/TOPO vector (Invitrogen), sequenced, then recombined into a yeast galactose-inducible vector, pDEST52 (Invitrogen), yielding pYDIS1.

***dis1* and *wrm* Allele Characterization**
PCR products that spanned the *DIS1* and *WRM* coding region were sequenced directly by using standard procedures. The *DIS1* and *WRM* templates and primer sequences are in Figure S4 (in the Supplemental Data). The reported Salk_010045 T-DNA insertion in the *ATARP3* gene was confirmed by PCR and sequencing, by using *DIS1* primers LP1: 5′-TGCTGAAATCGCTTGAAAAG-3′ and RP1: 5′-CTGACCAGTCTTTGGCGTTT-3′ and the T-DNA-specific primer 5′-CCGTCTCACTGGTGAAAAGAA-3′. The *WRM* coding region was sequenced by using 12 forward primers (WRM-F1–WRM-F12) and 12 reverse primers (WRM-R1–WRM-R12) (see Figures S3C and S3D). The reported Salk_003448 T-DNA insertion in the *ATARP2* gene was confirmed by PCR using two *WRM*-specific primers, LP1: 5′-GCTGCTTTTTGTTTGTCGAA-3′ and RP1: 5′-AGAGCAAGTCTCCCCACCAA-3′ and the T-DNA-specific primer listed above.

RT-PCR
Total RNA for RT-PCR was isolated by using the RNeasy from Qiagen. Five micrograms total RNA was treated with 5 U RQ1 RNase-Free DNase (Promega). For the first strand cDNA synthesis, 1 μg total RNA was used and was then primed with a mixture of random

hexanucleotides at a final concentration of 20 ng μl^{-1} (New England Biolabs) and reverse transcribed with 8 U μl^{-1} M-MLV (Invitrogen). Thereafter, 1/25 volume of the cDNA was used as a template for PCR.

Supplemental Data
Supplemental Data including amino acid sequence alignments between *DIS*, *WRM*, and known ARPs; example confocal images of trichome branches that were used to quantitate relative F-actin amounts; and a detailed description of the oligonucleotide primers that were used for *dis1* and *wrm* allele sequencing are available at http://www.current-biology.com/cgi/content/full/13/15/1341/DC1/.

References

1. Staiger, C.J. (2000). Signaling to the actin cytoskeleton in plants. Annu. Rev. Plant Physiol. Plant Mol. Biol. *51*, 257–288.
2. Beilstein, M., and Szymanski, D. (2003). Cytoskeletal requirements during *Arabidopsis* trichome development. In The Plant Cytoskeleton in Cell Differentiation and Development, P. Hussey, ed. (Oxford, UK: Blackwell), in press.
3. Welch, M., and Mullins, D. (2002). Cellular control of actin nucleation. Annu. Rev. Cell Dev. Biol. *18*, 247–288.
4. Szymanski, D.B., Marks, M.D., and Wick, S.M. (1999). Organized F-actin is essential for normal trichome morphogenesis in *Arabidopsis*. Plant Cell *11*, 2331–2347.
5. Schwab, B., Mathur, J., Saedler, R.R., Schwarz, H., Frey, B., Scheidegger, C., and Hulskamp, M. (2003). Regulation of cell expansion by the *DISTORTED* genes in *Arabidopsis thaliana*: actin controls the spatial organization of microtubules. Mol. Genet. Genome *269*, 350–360.
6. Qiu, J.L., Jilk, R., Marks, M.D., and Szymanski, D.B. (2002). The *Arabidopsis SPIKE1* gene is required for normal cell shape control and tissue development. Plant Cell *14*, 101–118.
7. McKinney, E.C., Kandasamy, M.K., and Meagher, R.B. (2002). *Arabidopsis* contains ancient classes of differentially expressed actin-related protein genes. Plant Physiol. *128*, 997–1007.
8. Baluska, F., Salaj, J., Mathur, J., Braun, M., Jasper, F., Samaj, J., Chua, N.H., Barlow, P.W., and Volkmann, D. (2000). Root hair formation: F-actin-dependent tip growth is initiated by local assembly of profilin-supported F-actin meshworks accumulated within expansin-enriched bulges. Dev. Biol. *227*, 618–632.
9. Feenstra, W.J. (1978). Contiguity of linkage groups I and IV as revealed by linkage relationship of two newly isolated markers *dis-1* and *dis-2*. Arab. Inf. Serv. *15*, 35–38.
10. Seki, M., Carninci, P., Nishiyama, Y., Hayashizaki, Y., and Shinozaki, K. (1998). High-efficiency cloning of *Arabidopsis* full-length cDNA by biotinylated CAP trapper. Plant J. *15*, 707–720.
11. Robinson, R., Turbedsky, K., Kaiser, D., Marchand, J.-B., Higgs, H., Choe, S., and Pollard, T. (2001). Crystal structure of Arp 2/3 complex. Science *294*, 1679–1684.
12. Kelleher, J.F., Atkinson, S.J., and Pollard, T.D. (1995). Sequences, structural models, and cellular localization of the actin-related proteins Arp2 and Arp3 from *Acanthamoeba*. J. Cell Biol. *131*, 385–397.

13. Lorenz, M., Popp, D., and Holmes, K.C. (1993). Refinement of the F-actin model against x-ray fiber diffraction data by the use of a directed mutation algorithm. J. Mol. Biol. *234*, 826–836.

14. Machesky, L.M., Reeves, E., Wientjes, F., Mattheyse, F.J., Grogan, A., Totty, N.F., Burlingame, A.L., Hsuan, J.J., and Segal, A.W. (1997). Mammalian actin-related protein 2/3 complex localizes to regions of lamellipodial protrusion and is composed of evolutionarily conserved proteins. Biochem. J. *328*, 105–112.

15. Insall, R., Müller-Taubenberger, A., Machesky, L., Köhler, J., Simmeth, E., Atkinson, S.J., Weber, I., and Gerisch, G. (2001). Dynamics of the *Dictyostelium* Arp2/3 complex in endocytosis, cytokinesis, and chemotaxis. Cell Motil. Cytoskeleton *50*, 115–128.

16. Welch, M.D., Iwamatsu, A., and Mitchison, T.J. (1997). Actin polymerization is induced by Arp2/3 protein complex at the surface of *Listeria monocytogenes*. Nature *385*, 265–269.

17. Winter, D., Choe, E., and Li, R. (1999). Genetic dissection of the budding yeast Arp 2/3 complex: a comparison of the *in vivo* and structural roles of individual subunits. Proc. Natl. Acad. Sci. USA *96*, 7288–7293.

18. Winter, D., Podtelejnikov, A.V., Mann, M., and Li, R. (1997). The complex containing actin-related proteins Arp2 and Arp3 is required for the motility and integrity of yeast actin patches. Curr. Biol. *7*, 519–529.

19. Szymanski, D.B. (2001). *Arabidopsis* trichome morphogenesis: a genetic approach to studying cytoskeletal function. J. Plant Growth Regul. *20*, 131–140.

20. Blanchoin, L., Amann, K.J., Higgs, H.N., Marchand, J.B., Kaiser, D.A., and Pollard, T.D. (2000). Direct observation of dendritic actin filament networks nucleated by Arp2/3 complex and WASP/Scar proteins. Nature *404*, 1007–1011.

21. Amann, K., and Pollard, T. (2001). Direct real-time observation of action filament branching mediated by Arp 2/3 complex using total internal reflection fluorescence microscopy. Proc. Natl. Acad. Sci. USA *98*, 15009–15013.

22. Mullins, D., and Pollard, T. (1999). Structure and function of the Arp 2/3 complex. Curr. Opin. Cell Biol. *9*, 244–249.

23. Schafer, D.A. (2002). Coupling actin dynamics and membrane dynamics during endocytosis. Curr. Opin. Cell Biol. *14*, 76–81.

24. Vignjevic, D., Yarar, D., Welch, M., Peloquin, J., Svitkina, T., and Borisy, G. (2003). Formation of filopodia-like bundles in vitro from a dendritic network. J. Cell Biol. *160*, 951–962.

25. Kovar, D.R., Staiger, C.J., Weaver, E.A., and McCurdy, D.W. (2000). AtFim1 is an actin filament crosslinking protein from *Arabidopsis thaliana*. Plant J. *24*, 625–636.

26. Klahre, U., Friederich, E., Kost, B., Louvard, D., and Chua, N.H. (2000). Villin-like actin-binding proteins are expressed ubiquitously in *Arabidopsis*. Plant Physiol. *122*, 35–48.

27. Hudson, A.M., and Cooley, L. (2002). A subset of dynamic actin rearrangements in *Drosophila* requires the Arp2/3 complex. J. Cell Biol. *156*, 677–687.

28. Lees-Miller, J.P., Henry, G., and Helfman, D.M. (1992). Identification of *act2*, an essential gene in the fission yeast *Schizosaccharomyces pombe* that encodes a protein related to actin. Proc. Natl. Acad. Sci. USA *89*, 80–83.

29. Pruyne, D., Evangelista, M., Yang, C., Bi, E., Zigmond, S.H., Bretscher, A., and Boone, C. (2002). Role of formins in actin assembly: nucleation and barbed-end association. Science *297*, 612–615.

30. Sagot, I., Klee, S.K., and Pellman, D. (2002). Yeast formins regulate cell polarity by controlling the assembly of actin cables. Nat. Cell Biol. *4*, 42–50.

31. Deeks, M.J., Hussey, P.J., and Davies, B. (2002). Formins: intermediates in signal-transduction cascades that affect cytoskeletal reorganization. Trends Plant Sci. *7*, 492–498.